Fusion Engineering and Design 85 (2010) 865–873

Contents lists available at ScienceDirect

Fusion Engineering and Design

journal homepage: www.elsevier.com/locate/fusengdes

# Lithium coatings on NSTX plasma facing components and its effects on boundary control, core plasma performance, and operation

H.W. Kugel[a,*], M.G. Bell[a], H. Schneider[a], J.P. Allain[b], R.E. Bell[a], R. Kaita[a], J. Kallman[a], S. Kaye[a], B.P. LeBlanc[a], D. Mansfield[a], R.E. Nygren[c], R. Maingi[d], J. Menard[a], D. Mueller[a], M. Ono[a], S. Paul[a], S. Gerhardt[a], R. Raman[e], S. Sabbagh[f], C.H. Skinner[a], V. Soukhanovskii[g], J. Timberlake[a], L.E. Zakharov[a], the NSTX Research Team

[a] Princeton Plasma Physics Laboratory, PO Box 451, Princeton, NJ 08543, USA
[b] Purdue University, School of Nuclear Engineering, West Lafayette, IN 47907, USA
[c] Sandia National Laboratories, Albuquerque, NM 87185, USA
[d] Oak Ridge National Laboratory, Oak Ridge, TN 37831, USA
[e] University of Washington, Seattle, WA 98195, USA
[f] Columbia University, New York, NY 10027, USA
[g] Lawrence Livermore National Laboratory, Livermore, CA 94551, USA

ARTICLE INFO

*Keywords:*
Lithium
Lithium wall fusion regime
Recycling
Plasma wall interactions
Divertors
Spherical torus

ABSTRACT

NSTX high power divertor plasma experiments have used in succession lithium pellet injection (LPI), evaporated lithium, and injected lithium powder to apply lithium coatings to graphite plasma facing components. In 2005, following the wall conditioning and LPI, discharges exhibited edge density reduction and performance improvements. Since 2006, first one, and now two lithium evaporators have been used routinely to evaporate lithium onto the lower divertor region at total rates of 10–70 mg/min for periods 5–10 min between discharges. Prior to each discharge, the evaporators are withdrawn behind shutters. Significant improvements in the performance of NBI heated divertor discharges resulting from these lithium depositions were observed. These evaporators are now used for more than 80% of NSTX discharges. Initial work with injecting fine lithium powder into the edge of NBI heated deuterium discharges yielded comparable changes in performance. Several operational issues encountered with lithium wall conditions, and the special procedures needed for vessel entry are discussed. The next step in this work is installation of a liquid lithium divertor surface on the outer part of the lower divertor.



## 1. Introduction

Density and impurity control, tritium and dust removal, and long-lifetime plasma facing components (PFCs) for diverted high power DT reactors are challenging technology problems. Replenishable liquid lithium PFCs show promise toward resolution of these challenges by providing a low-*Z*, pumping, self-healing plasma facing surface [1–3], and enabling a lithium wall fusion regime [4]. Preliminary work indicates that the use of liquid lithium as a PFC can help to integrate four important potential benefits for fusion: (a) divertor pumping over a large surface area compatible with high flux expansion solutions for power exhaust, together with high temperature low density plasma edge conditions, (b) improved confinement [5,6], (c) reduction or elimination of edge localized modes (ELMs) [7–9], and (d) high-heat flux handling [2,10,11].

### 1.1. National Spherical Torus Experiment lithium research

The National Spherical Torus Experiment (NSTX) [12,13] has been investigating solid lithium (Li) coatings for density and impurity control [5–7]. In NSTX, recycling of deuterium species from plasma contact with ATJ graphite surfaces contributes to a secular density rise observed in most H-mode, neutral beam injection (NBI) heated plasmas. Lithium has the potential for control of this density rise due to its ability to absorb the atomic and ionic deuterium efflux through the formation of lithium–deuteride and lithiated compounds [14], which sequesters deuterium, making it unavailable for recycling. Due to the range of deuterium in lithium, and the immobility of the lithium–deuteride formed in solid lithium, the absorption can saturate in the near surface layer [15], limiting the deuterium pumping capability of solid lithium. Subsequent recoating can replenish the surface with fresh lithium. Liquid lithium on

* Corresponding author. Tel.: +1 609 243 3146; fax: +1 609 243 3248.
*E-mail address:* hkugel@pppl.gov (H.W. Kugel).

0920-3796/$ – see front matter © 2010 Elsevier B.V. All rights reserved.
doi:10.1016/j.fusengdes.2010.04.004

the other hand has a much higher capacity for sequestering deuterium [16] because lithium–deuteride is more mobile in liquid lithium. In addition, it has potential for reactor applications [1–4]. Motivated by the long range potential of lithium PFCs, NSTX has been investigating lithium pellet injection and lithium evaporation for density and impurity control as part of a phased, three-part approach to lithium PFCs: first (i) lithium pellet injection [5], then (ii) lithium evaporators [6–8] and recently lithium powder [8], and finally (iii) a liquid lithium divertor [17,18]. This staged approach is allowing NSTX control systems, diagnostics, and research to be adapted to the evolving lithium technology.

## 2. Solid lithium coatings on graphite

In NSTX, the range of the 500–2000 eV deuterium efflux incident on lithium is 100–250 nm [15]. In the case of lithium coatings thicker than the range of the incident deuterium, lithium pumping via the formation of lithium–deuteride is restricted to a relatively thin surface region that can be quickly saturated by incident ion and neutral deuterium flux. This depletes the uncombined lithium available for lithium–deuteride formation. Also, lithium interactions with the NSTX residual vacuum constituents ($H_2O$, CO, and $CO_2$) yield surface accumulations of LiOH, $Li_2O$, and $Li_2CO_3$ which further decrease the amount of lithium available for deuteride formation. In addition, lithium can diffuse into relatively pure graphite and become unavailable at the surface for lithium–deuteride formation [19]. In NSTX, the diffusion of lithium was measured for the mature ATJ graphite divertor tiles to be limited to a few microns [19]. In addition, in the case of lithium coating thicknesses, less than the range of the incident deuterium, the lithium pumping efficiency is reduced as some incident particles are able to pass through the coating. Lithium coatings, for example, resulting from the injection of lithium pellets of a few mg deposited over 2 $m^2$ results in coating thicknesses of less than 30 nm which is significantly less than the 250 nm range.

In NSTX, the above effects have necessitated the continual deposition of fresh lithium between discharges to maintain active lithium pumping wall conditions.

### 2.1. Solid lithium coatings less than the range of incident deuterium in limiter and divertor experiments

Initially, TFTR obtained reduced recycling and significantly enhanced fusion performance by transitioning to a "supershot" regime. This was done by thoroughly degassing the inner toroidal limiter via about 40 helium conditioning discharges to obtain pumping by the graphite limiter. This graphite pumping state yielded the initial noteworthy fusion power results; however, the additional application of lithium deposition on the limiter, further enhanced limiter pumping, and yielded the very highest TFTR fusion power discharges [20]. TFTR also demonstrated that lithium deposition would not yield a performance enhancement without thorough limiter degassing beforehand. This can be understood as due to reactions of the freshly deposited lithium with fuel gas absorbed in the graphite, thereby making the relatively small amount of lithium unavailable for the pumping of subsequent deuterium efflux. Since TFTR, lithium pellet injection (LPI) was applied directly into normally fueled, diverted C-MOD, DIII-D, TdeV, and NSTX plasmas involving a variety of heating methods, but without thorough wall degassing, and confirmed that no performance improvement occurred other than a small decrease in core impurities.

#### 2.1.1. NSTX LPI with degassed PFCs

NSTX LPI experiments with thoroughly degassed graphite surfaces obtained a reduction in recycling, and made contact with the

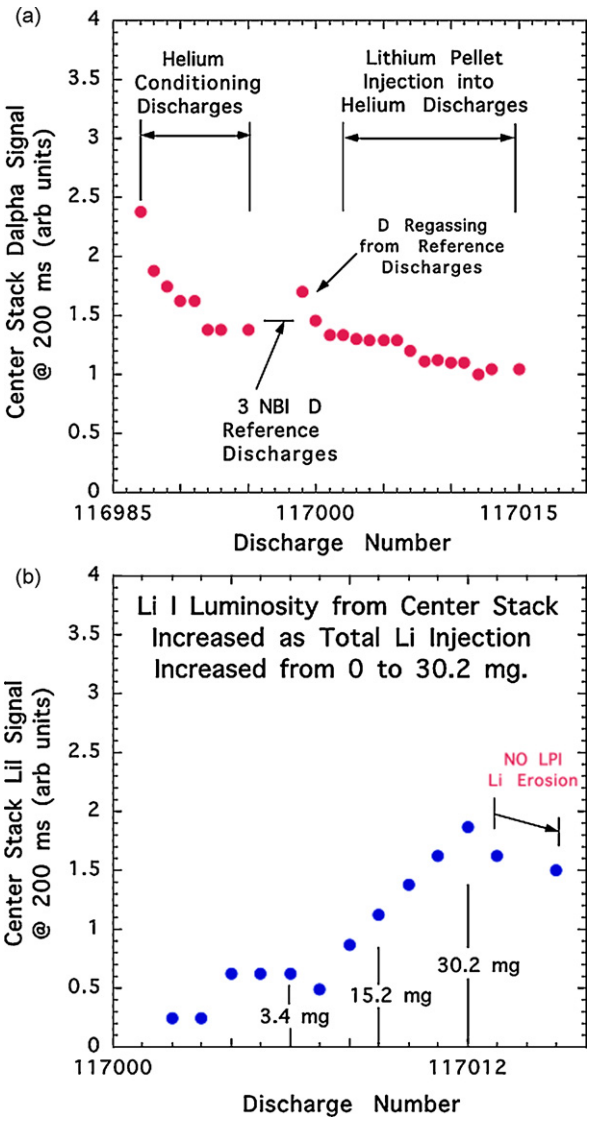


**Fig. 1.** (a) $D\alpha$ luminosity from the Center Stack region decreased during the helium conditioning as the discharge number increased and (b) the Li I luminosity increased.

TFTR performance enhancement results following lithium deposition on thoroughly degassed plasma wetted surfaces. The NSTX Center Stack provides an inner toroidal limiter during plasma startup and for toroidally limited plasmas. Ohmic helium, Center Stack Limited (CSL) discharges, and lower single null (LSN) diverted conditioning discharges were used to degas the Center Stack and the lower divertor. Fig. 1a shows how the $D\alpha$ luminosity indicates that although most of the degassing had been completed in about 8 discharges, it continued to decrease at a much lower rate, possibly due, in part, to mild recycling from distant main chamber surfaces. Three NBI reference discharges were then applied to test the conditioning of the limiting surface which was found to be satisfactory for LPI to begin. Then, LPI was started using 12 helium ohmic discharges, 9 with injection of either 1.7, 3.4, or 5.0 mg pellets at velocities of about 80–120 m/s. A lower rate of decrease in residual $D\alpha$ luminosity continued during this LPI deposition sequence into helium discharges. Shown in Fig. 1b is how the Li I luminosity from the Center Stack increased as total lithium injection increased to 30.2 mg. After completion of this LPI sequence, which deposited lithium on the Center Stack, deuterium reference discharges were taken to test for a reduction in recycling. Fig. 2 shows a 2 mg lithium pellet injected at 120 m/s into a helium ohmic discharge. At dis-

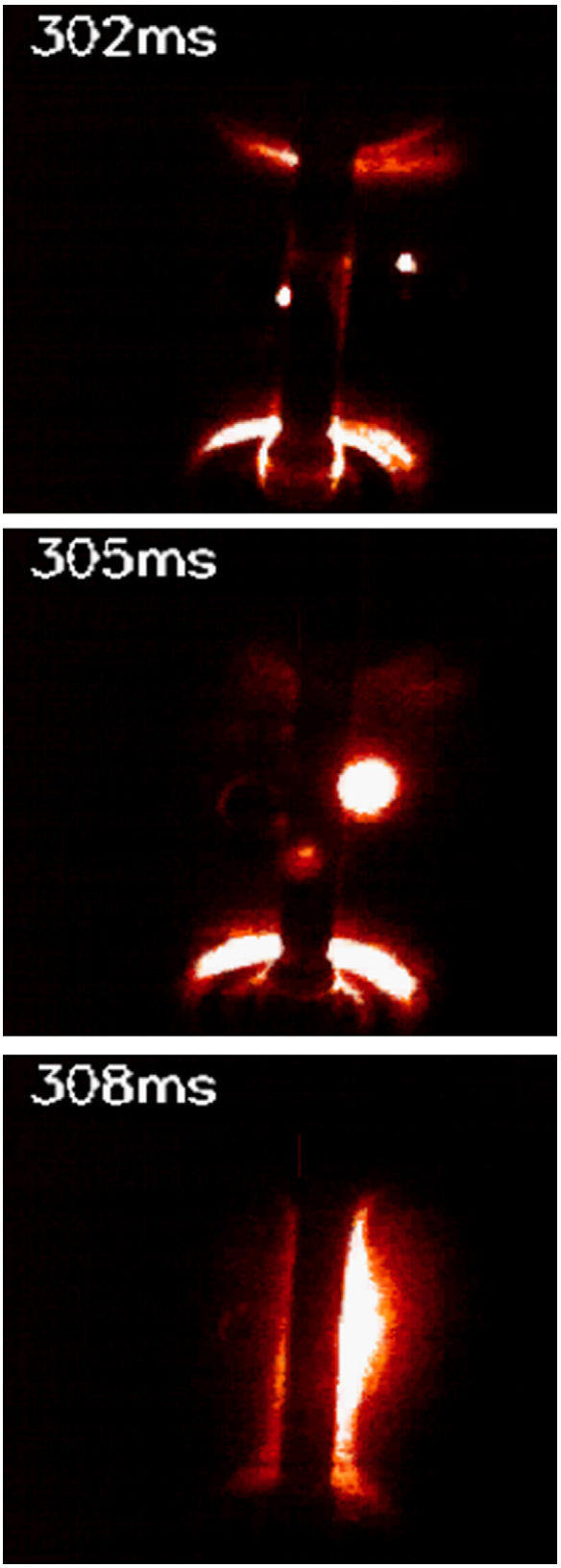


**Fig. 2.** Plasma TV photo of a 2 mg lithium pellet injected into a He ohmic discharge. At discharge time 302 ms, it enters the plasma and proceeds toward the Center Stack. At 305 ms, the lithium plasmoid is midway toward the Center Stack, and at 308 ms, it collides.

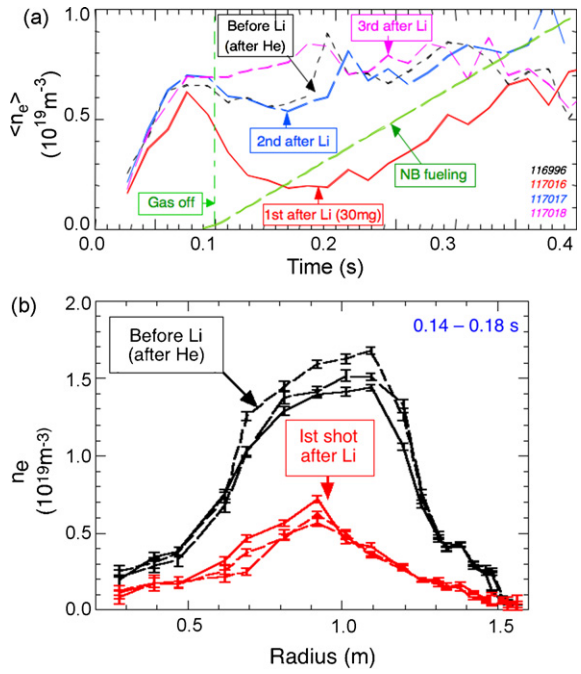


**Fig. 3.** (a) Waveforms for first CSL *D* discharge following this lithium deposition sequence and (b) the change in density profile after LPI.

charge time 302 ms, it enters the plasma and proceeds toward the Center Stack. At 305 ms, the lithium plasmoid is midway toward the Center Stack, and at 308 ms, it collides with it. Shown in Fig. 3a for the first discharge following this lithium deposition sequence is the density decrease that occurred as a result of the decrease in recycling. The pumping effect of the deposited lithium decreased with the subsequent discharge and disappeared by the 3rd discharge. Fig. 3b shows the change in density profile after LPI. Similar results were obtained following degassing of the lower divertor surface using diverted helium ohmic discharges followed by LPI. Fig. 3a illustrates the need for a thorough degassing of graphite plasma wetted surfaces when using thin lithium coatings. These results demonstrated the effectiveness of lithium edge pumping. Subsequently, the benefits of maintaining this edge pumping capability beyond 2–3 normal discharges motivated the development of an evaporation method for investigating the characteristics of thicker solid lithium coatings.

## 3. Solid lithium coatings greater than the range of incident deuterium in divertor experiments

As discussed above (Section 2.1), the deuterium ion and neutral pumping capacity of thicker solid lithium coatings are limited by the 100–250 nm range of deuterium efflux in lithium [15]. However, thicker coating applications on the divertor region, i.e., greater than the range of incident deuterium ions, depending on the application technique can provide more pumping capacity by extending thicker depositions to far chamber regions. In addition, in laboratory experiments thick coatings on stainless steel substrates have been found to be able saturate reactions with surface impurities, thereby allowing subsequently deposited lithium ions to provide an active lithium coating.

### 3.1. NSTX lithium evaporation techniques

NSTX has been applying thick solid lithium coatings to the lower divertor region since 2007. In 2009, about 80% of the experiments used these coatings. Fig. 4a shows a schematic diagram of one of

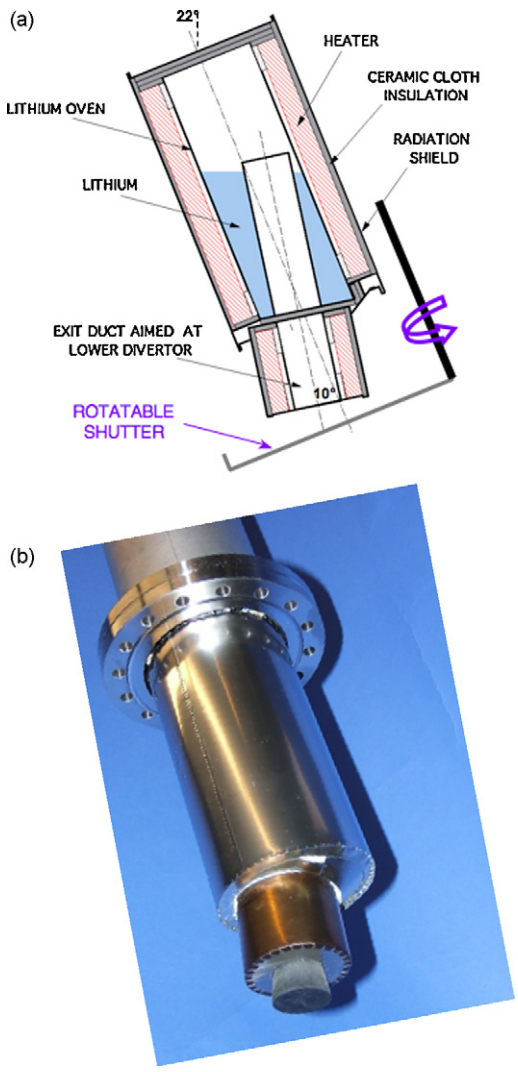


**Fig. 4.** (a) Schematic diagram of the Lithium EvaporatoR (LITER) with its rotatable lithium shutter shown in the position that stops lithium deposition during HeGDC and plasma discharges and (b) photograph of the unit loaded with lithium under argon and sealed with a rubber stopper which is removed prior to installation (shutter not shown).

the two identical Lithium EvaporatoR (LITER) units, used to apply these coatings. The liquid lithium capacity of each oven is 90 g. The main probe and oven axis are inclined 22° from the vertical to allow passage through the NSTX upper divertor ports. The oven output aperture is inclined an additional 10° downward from the probe drive axis so as to aim at the inner lower divertor region. The stainless steel (304-SS) oven is clad with resistive wire heaters. The output aperture has a separate heater that is operated at a higher temperature than the main oven so as to prevent lithium condensate build up. The heaters are clad with alumina-based, ceramic cloth covered by an outer 304-SS radiation shield. The LITER oven temperatures are monitored and controlled using type-K thermocouples. The ovens are operated in the temperature range 550–640 °C to provide Li evaporation rates of 5–70 mg/min, which are typically applied for 10 min between discharges. Shown also in Fig. 4a, in front of the output aperture is a rotatable Li shutter which closes, and interrupts the lithium vapor stream, when the diagnostic window shutters are open during a discharge. Shown in Fig. 4b is a photograph of the oven mounted on the insertion probe. Fig. 5 shows a schematic diagram of the poloidal cross-section of NSTX and the locations of two LITERs at toroidal angles 165° and

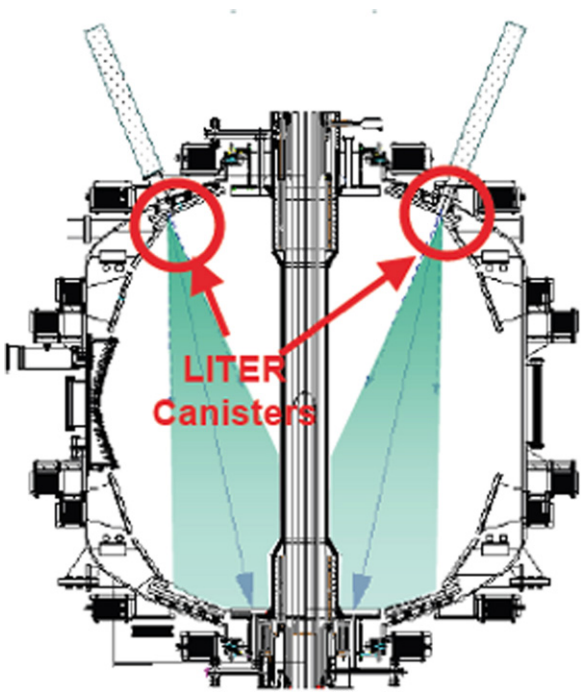


**Fig. 5.** Schematic diagram of the poloidal cross-section of NSTX and the locations of two LITERS at toroidal angles 165° and 315°, and the LITER central axes aimed at the lower divertor. The shaded regions indicate the measured Gaussian half-angle at the 1/e intensity of the measured evaporated lithium angular distributions.

315°, and the LITER central axes aimed at the lower divertor. The shaded regions indicate the measured half-angle of the roughly Gaussian measured angular distribution at the 1/e intensity. Fig. 6a illustrates the timing sequence for LITER deposition prior to the installation of the shutters. The machine discharge repetition time was about every 15 min. Helium glow-discharge cleaning (HeGDC) was applied between discharges for up to 6.5 min as required by the experiment in progress. Due to the thermal inertia of the LITER units, they were unable to cool down during this short time, and hence, they were operated to continuously evaporate during the 12–15 min between discharges. The disadvantages of this approach were two-fold. First the diagnostic windows received some "off target" lithium deposition during the discharge, and secondly, the HeGDC caused lithium to ionize and to be codeposited with helium

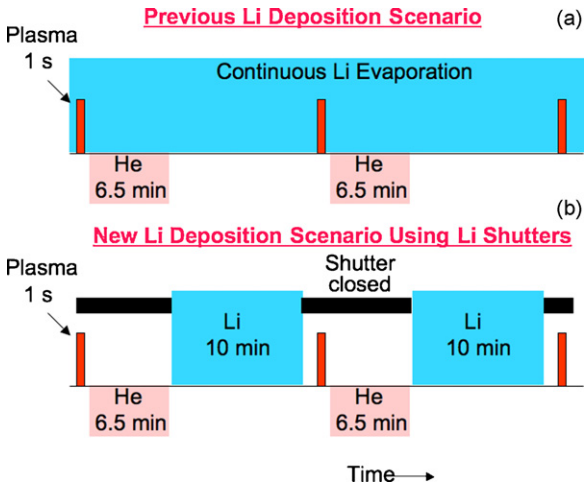


**Fig. 6.** (a) Timing sequence for LITER deposition prior to the installation of the shutters and (b) the respective lithium shutters closed during HeGDC and plasma discharges.

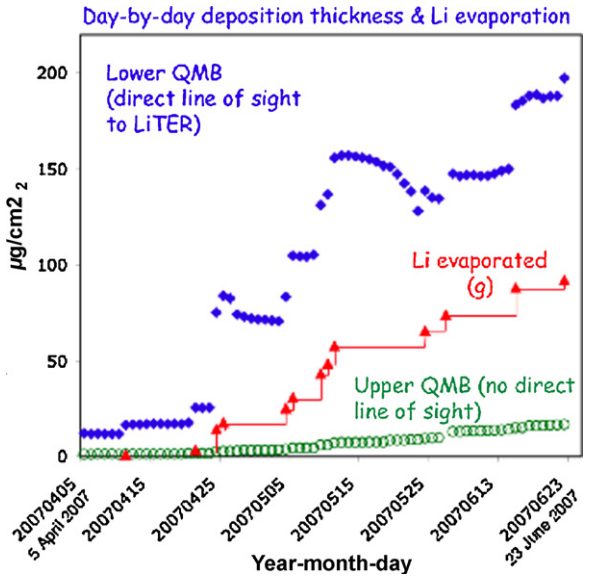


**Fig. 7.** The signals of the lower quartz deposition monitor (QDM), in direct line of sight of LITER (blue), and the upper QDM, not in direct line of sight of LITER (green, offset by 20 $\mu g/cm^2$) increase as the total evaporated Li increases (red). Dates of 10 g boronization are also shown by triangles.

incident on the PFC surface. This trapped helium which slowly diffused out on a time-scale of 10 s of minutes and resulted in helium dilution of the subsequent deuterium plasma. Since 2008, the evaporators have been equipped with shutters (Fig. 4a), to block the output lithium stream during HeGDC and during discharges. Fig. 6b illustrates the present lithium deposition scenario using lithium shutters. During each discharge, the LITER units are parked at the outer wall with their shutters closed. Then, if desired for the experiment in progress, HeGDC is applied for 2–6.5 min. After HeGDC is completed, the lithium shutters on the LITER units are opened, and the units are reinserted from the outer wall to their operating positions near the major radius of the graphite PFCs for the evaporation. About 30 s before the next discharge, the LITER probes are withdrawn to their parked position and their lithium shutters are closed. This sequence is repeated automatically under computer control for each discharge during the operating day. Shown in Fig. 7 are how the signals of the lower quartz deposition monitor (QDM) in direct line of sight of LITER, and that of the upper QDM not in direct line of sight of LITER increase as the total evaporated lithium increases. The decreases in the integrated lower QDM signal between discharges may be due to structural instability of thick lithium coatings on the QDM crystal. The increase in the signal of the upper QDM may be due to the transport of eroded lithium by the plasma.

### 3.2. *NSTX results following application solid lithium coatings greater than the range of incident deuterium*

NSTX thick solid lithium coatings have been applied to both well-conditioned, relatively oxygen-free, degassed divertor graphite PFCs, and also to relatively unconditioned divertor graphite PFCs exhibiting high oxygen desorption. The well-conditioned, low oxygen conditions were achieved by first removing oxides, as much as possible, from the PFCs prior to evacuation (discussed in Section 5 below) and after evacuation by bakeout of the PFCs at 350 °C for 2 weeks, followed by deuterated trimethylboron (TMB) boronization, and 6 h of HeGDC [7]. In the case of the application of thick lithium coatings (>250 nm) to unconditioned divertor graphite PFCs exhibiting high oxygen desorption, the impurity gettering effect of these coatings was found to accelerate the recovery of good lithium wall conditions.

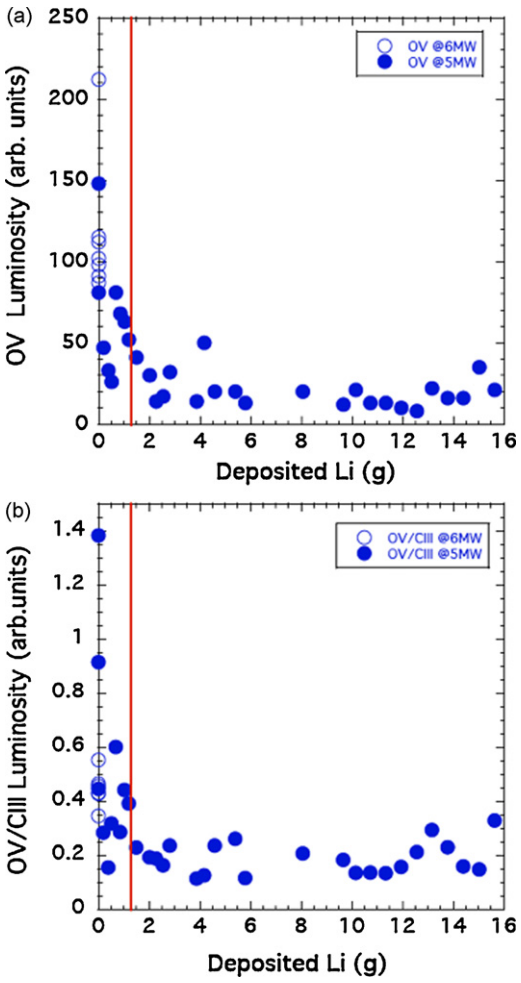


**Fig. 8.** (a) OV and (b) OV/CIII luminosities decreased as lithium deposition increased. The vertical red line indicates the lithium deposition yielding a thickness comparable to the 250 nm range of *D* in lithium.

This can be understood if as the initial lithium depositions on unconditioned graphite reacted to bind volatile surface impurities into lithium compounds, these were increasing covered by fresh lithium. This resulted in low impurity, good plasma wall conditions, and thereby allowed more of the fresh lithium applied between discharges to be available for deuterium edge pumping during discharges. Fig. 8 shows for relatively unconditioned divertor graphite PFCs exhibiting high oxygen desorption, how the (a) OV luminosity and (b) OV/CIII ratio in *D* plasmas decreased as lithium deposition on the lower divertor increased. At ~1.3 g total lithium deposition, average lithium deposition thickness over lower 25% of vessel becomes comparable to the 250 nm range of incident *D*, and the OV and OV/CIII luminosities stop decreasing. Thereafter, the relatively constant OV and OV/CIII ratios as lithium deposition over lower divertor increased may be due to oxygen contributions from the main chamber regions of partially coated graphite (e.g., upper and outer vessel hardware). Shown in Fig. 9 is how the deuterium discharge performance responded quickly to the transition to lithium wall conditions. Fig. 10 shows waveforms exhibiting how for relatively oxygen-free pre-lithium wall conditions, a thick solid lithium coating reduces deuterium recycling, suppresses ELMs [9,21], increases stored energy, and improves confinement. Note, however, that with improved confinement and without ELMs, impurity accumulation increases radiated power and $Z_{eff}$. In regard to impurity accumulation, quantitative measurements described below (Fig. 13) of $C^{6+}$, $Li^{3+}$ with charge-exchange recombination

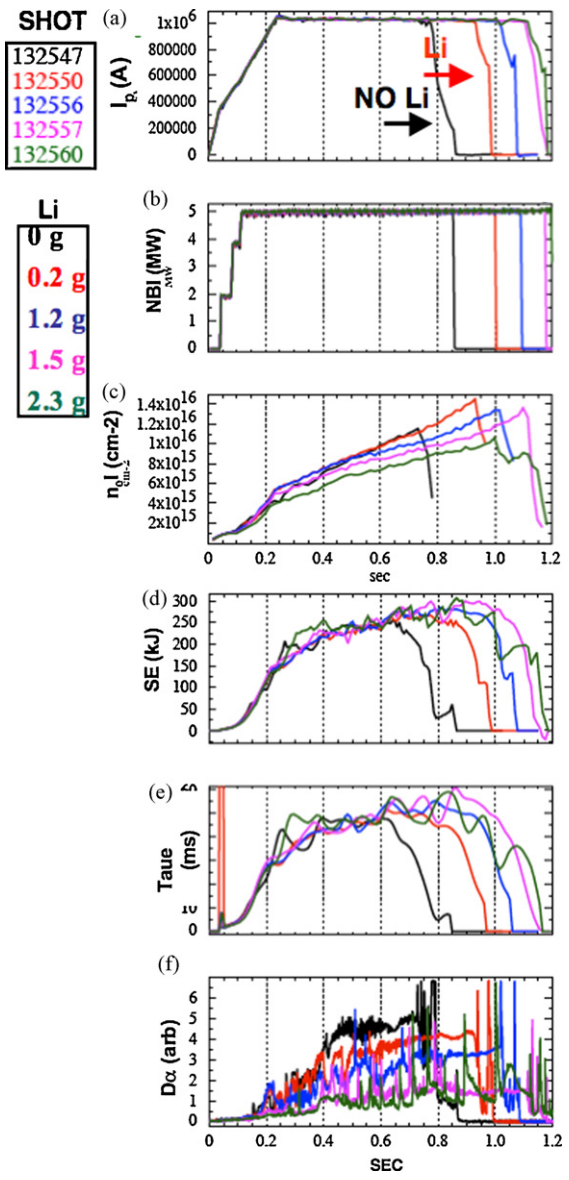


**Fig. 9.** Starting from poor wall conditions with relatively large oxygen content, deuterium discharge performance responded quickly as the lithium coating thickness increased and NSTX transitioned to lithium wall conditions.

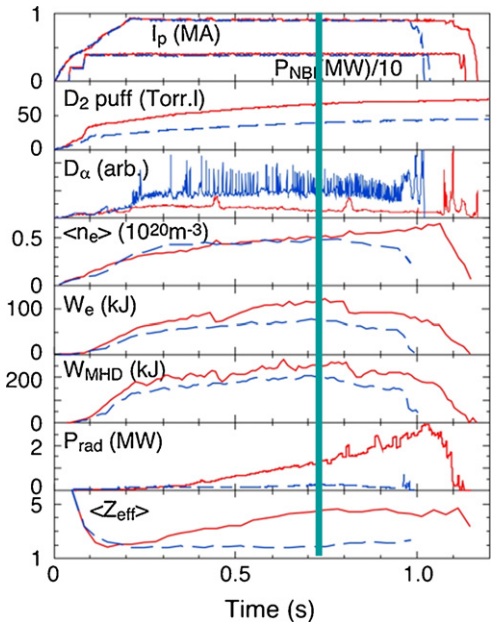


**Fig. 10.** Reference waveforms for relatively oxygen-free pre-lithium wall conditions (black). After 260 mg lithium deposition (red) deuterium recycling reduced, ELMs suppressed, stored energy increased, confinement improves. Refer to Fig. 11.

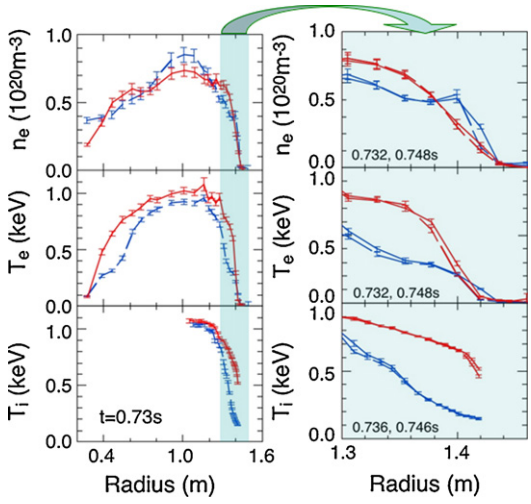


**Fig. 11.** Radial profiles before (blue) and after 260 mg lithium deposition (red) at the time referenced by the vertical line in Fig. 10 at 0.72 s for relatively oxygen-free pre-lithium wall condition.

spectroscopy indicate that the core carbon to lithium density ratio is 30–100. One method to eliminate this impurity accumulation is to introduce controlled ELMs via application of 3D fields [22]. Shown in Fig. 11 are the radial profiles before (blue) and after 260 mg lithium deposition (red) at the time referenced by the vertical line in Fig. 10 (0.72 s) for relatively oxygen-free pre-lithium wall condition. The radial density and temperature profiles show that the transition to lithium wall conditions produced high temperature low density plasma edge conditions. Fig. 12 shows a database of electron stored energy ($W_e$) versus total stored energy ($W_{MHD}$) for *D* reference plasmas immediately following lithium deposition, and for *D* reference plasmas prior to lithium deposition. The increase in stored energy is mostly in the electron channel. Shown in Fig. 13 is how the lithium concentration in plasmas remains low but carbon concentration rises with lithium coating. As noted above, this rise in plasma core carbon concentration is a consequence of the improvement in the particle confinement (deuterium and impurities), and ELMS-free discharges due to lithium wall conditions [9,13]. The application of external fields to induce ELMs reduces core impu-

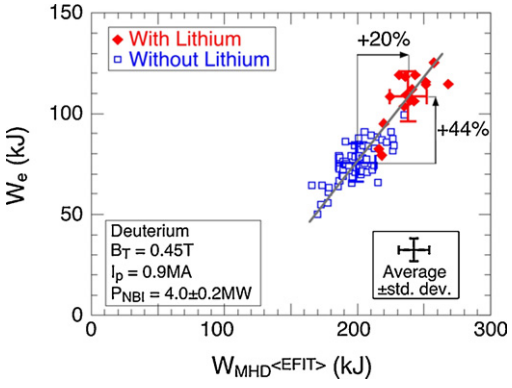


**Fig. 12.** Electron stored energy (kJ) versus total stored energy as determined from EFIT02 (an equilibrium analysis constrained by external magnetics, electron profile shape, and diamagnetic flux).

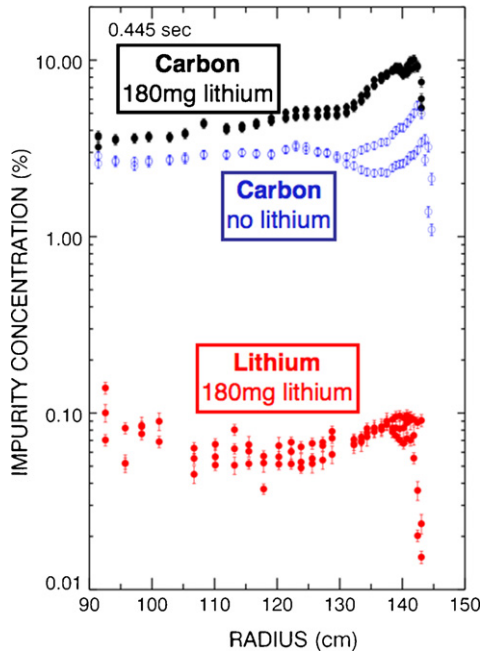


**Fig. 13.** The results of charge-exchange recombination measurements for thick lithium coatings show that absolute lithium concentration in plasmas remains low but carbon concentration rises with lithium coating.

rity concentrations and the associated core impurity radiation [22]. The profiles early in the discharge for both carbon and lithium are hollow but fill in as the discharge progresses. Core lithium levels are about 0.1%, whereas, the core C levels are of order 3% of the core density. Fig. 14 shows how the broader $T_e$ profiles with lithium coating reduce both inductive and resistive poloidal flux consumption. This is a critical issue for the development of neutral beam current drive for low-aspect ratio tokamaks [13]. This reduction occurs despite an increase in $\langle Z_{eff} \rangle$ in ELM-free H-modes after lithium coating. An additional operating benefit, namely an increased number of discharges per day results from the gradual reduction, and elimination of HeGDC between discharges that becomes possible as the lithium coating becomes thicker. These results demonstrated the effectiveness of lithium edge pumping. However, while the plasma performance benefits that accrued from the deposition of thick solid lithium coatings, and extended the initial results obtained with thin solid coatings, the resultant higher stored energies, hotter edge temperatures, and longer pulse lengths have not allowed the edge pumping effectiveness to be maintained

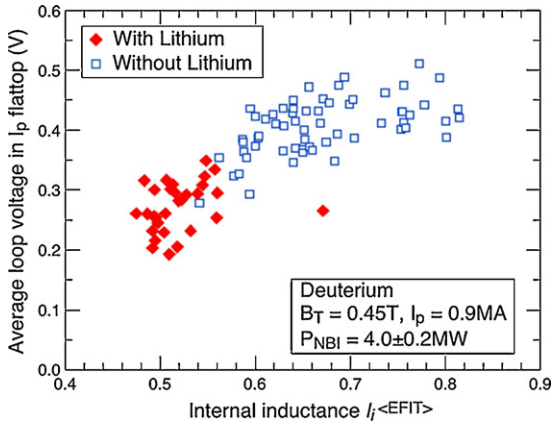


**Fig. 14.** Average loop voltage versus internal inductance of discharges prior to lithium coating (blue) and after lithium coating (red).

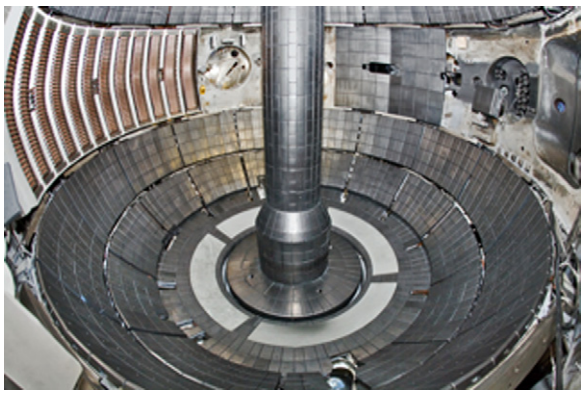

**Fig. 15.** Photo of liquid lithium divertor (LLD-1) installed 2010 near the inner edge of the outer divertor, It consists of four 80° sections, each 20 cm wide in the radial direction. Each section is separated by a row of graphite diagnostic tiles containing magnetic sensors, thermocouples, Langmuir probes and bias electrodes.

without constant between discharge evaporation to maintain stable lithium PFC conditions. The benefits of maintaining this lithium edge pumping capability for increasingly longer pulse higher power discharges has motivated work toward extending this capability.

## 4. Liquid lithium divertor

The next phase of NSTX lithium work is to extend the results obtained with thick solid lithium coatings using a liquid lithium divertor (LLD-1). The LLD-1 physics design goals are to achieve increased neutral beam current drive by maintaining the density at or below $n_e \sim 5 \times 10^{19}$ m$^{-3}$ at $I_p$ = 700 kA. This represents about a 15–25% decrease in density from the present experiments. Key design features of the LLD-1 include providing a surface allowing liquid lithium to flow across it (wetting capability), sufficient surface area for surface tension to hold thin liquid lithium films in the presence of J × B forces, and minimal temperature rate of rise of the lithium plasma facing surface via rapid heat transfer from lithium to the copper base.

### 4.1. Liquid lithium divertor geometry

In the work described above, the LITER evaporators were used to provide thicker solid lithium coatings over a broad region of the lower divertor graphite PFCs. Operation with LLD-1 will change the experimental geometry by replacing a 20 cm wide toroidal conic section of outer divertor graphite PFCs with heated porous molybdenum plates [17,18]. Shown in Fig. 15 is a recent photo of LLD-1 installed near the inner edge of the outer divertor. It consists of four 80° sections, each 20 cm wide in the radial direction. The plasma facing surface is a thin layer of 0.165 mm molybdenum plasma-sprayed with a 45% porosity on to a 0.25 mm stainless steel barrier brazed to a 2.2 cm copper baseplate. Each toroidal section is fastened at its corners to the divertor copper baseplate with fasteners providing structural support, and electrical isolation, and allowing thermal expansion. Each toroidal section is electrically grounded to vessel at one mid-segment location to control eddy currents. Electrical heaters and gas cooling lines will be used to maintain a temperature in the range 200–400 °C. Each section is separated by graphite tiles containing at various locations magnetic sensors, thermocouples, Langmuir probes, and bias electrodes. Initially, LLD-1 and the lower divertor graphite PFCs will be lithium coated using the LITER units. Later LLD embodiments may involve a flowing lithium fill system. High-triangularity diverted discharges with the outer strike point incident inboard of the LLD-1 will be pumped, via power flowing along open field lines incident on LLD-

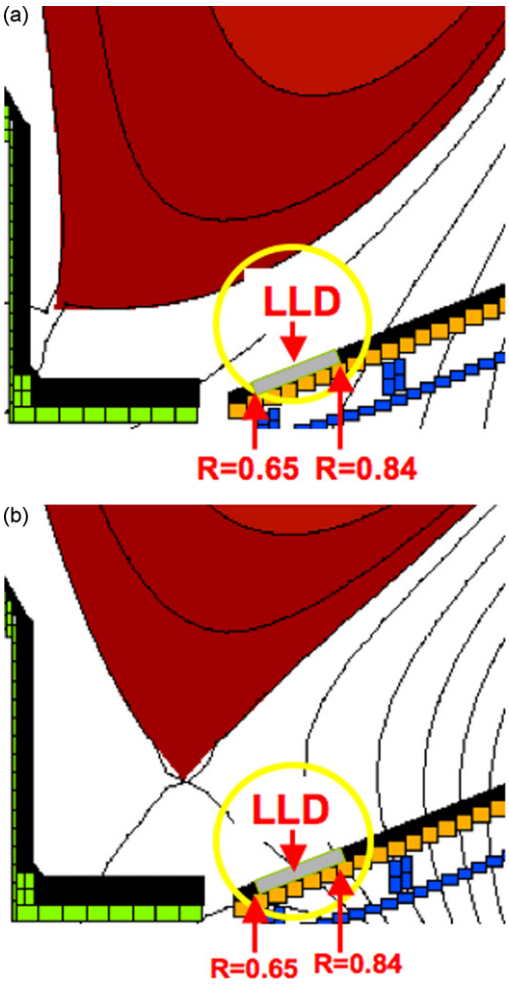


**Fig. 16.** (a) High-triangularity lower single null diverted plasma with strike point on inner divertor and open field lines incident on the LLD, and (b) medium triangularity of the plasma with most of its deuterium efflux onto the LLD.

1. This is due to the high flux expansion factor (15–20×) in NSTX between the midplane and divertor (Fig. 16a). Medium triangularity diverted discharges with the outer strike point incident directly on LLD-1 will be pumped through absorption (Fig. 16b). The capability to apply this range of diverted discharge topologies will allow tests of the potential benefits of liquid lithium divertor for integrating high plasma and PSI performance. In particular, this will test flexible broad area pumping to reduce density for increased neutral beam current drive capability.

## 5. PFC maintenance after extensive lithium operation

Since the first lithium experiments in 2005, annual NSTX lithium usage has increased until in 2009 it reached about 600 g and was employed in over 80% of the experimentally specified discharges. Under NSTX vacuum conditions, with a base pressures in the range of about $(3–5)\times10^{-8}$ Torr, this annual lithium deposition reacts slowly with the residual vacuum constituents ($H_2O$, CO, $CO_2$) to form lithium compounds containing oxygen, predominantly LiOH, and to a lesser extent $Li_2O$ and $Li_2CO_3$ [14]. After an annual 12–18 week experimental campaign, NSTX is vented with the local atmosphere, and purged with humidified air for at least 1 week prior to the first personnel entry. This procedure converts any residual active lithium and LiOH to mostly $Li_2CO_3$. The vessel is then entered by a team of 3 to perform inspection, sample collection and photography. Shown in Fig. 17 is a wide angle photograph of

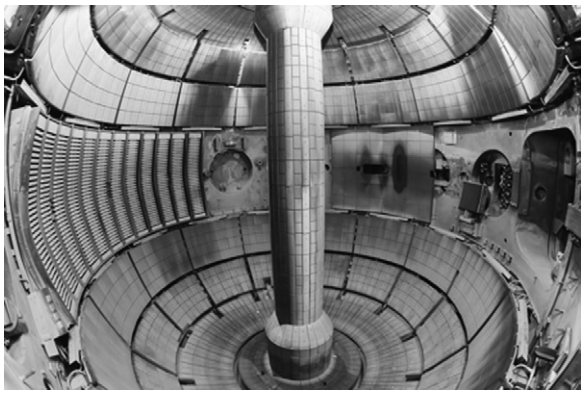

**Fig. 17.** Wide angle photograph of NSTX after venting following 2009 experimental campaign showing the extensive white coating of lithium carbonate on all surfaces.

the interior of NSTX after venting and prior to personnel entering the vessel. The white coating on all surfaces is lithium carbonate ($Li_2CO_3$). After the initial inspection work is completed, all interior surfaces are washed with deionized water and wet lint-free cloths. All graphite tiles are then sanded with Scotchbrite (an abrasive material) to remove $Li_2CO_3$ and oxides. All other metal surfaces are washed with a 5% solution of acetic acid ($CH_3COOH$ in common vinegar) to convert hard ceramic $Li_2CO_3$ to water soluble lithium acetate ($LiC_2H_3O_2$) and removal with wet lint-free cloths. The goal of these PFC cleanup procedures is to remove the oxygen bound in lithium compounds. This is very important because if, for example, all 600 g of lithium coating were converted $Li_2CO_3$, this lithium binds about 2 kg of oxygen in the form of a hard, white, nonconducting ceramic coating on all plasma facing surfaces. This oxygen if not removed is eroded by plasma interactions, and results in short, highly-radiative, high impurity content discharges.

## 6. Discussion and conclusions

More than a decade of research has pointed to the merits and reactor relevance of replenishable liquid lithium walls for providing a pumping, impurity flushing, low-*Z*, self-healing plasma facing surface [1–3], and enabling a lithium wall fusion regime [4]. NSTX lithium experiments are the first extension of this work to high beta, high power, long pulse, NBI conditions in a spherical torus with divertor *P*/*R* ratios of 28–56 MW/m and eventually higher. This work has been pursued in a measured manner, allowing NSTX control systems, diagnostics, and research to be adapted to the lithium PFC conditions. NSTX experiments with LPI, evaporated lithium coatings, and lithium powder have found that relatively thin lithium coatings (<250 nm) increased the plasma current pulse length relative to the before-lithium reference discharges, caused earlier H-mode transitions, caused significant density reduction in the early part of discharges calling for more fueling, increased electron temperature, electron stored energy and confinement time, and reduced OV/CIII impurity ratios. As the solid lithium coating thickness increases (>250 nm), high elongation H-mode discharges became ELM-free. Eventually the HeGDC previously routinely employed between plasma shots, was eliminated, allowing an increased duty cycle.

Characterization of the plasma performance regime achieved with the liquid lithium divertor for diverted discharge topologies ranging from high to medium triangularity discharges will allow tests of the potential benefits of liquid lithium divertors for integrating high plasma and plasma surface interaction performance, and, in particular, will test flexible broad area pumping to reduce density for increased neutral beam current drive capability. This work foresees and motivates research and development needed to

obtain reactor relevant designs for high power, long pulse, liquid lithium surfaces.

## Acknowledgments

This work is supported by United States Department of Energy (US DOE) Contracts DE-AC02-09CH11466 (PPPL), DE-AC05-00OR22725 (ORNL), and those of Lawrence Livermore National Laboratory in part under Contract W-7405-Eng-48 and in part under Contract DE-AC52-07NA27344, and that of Sandia, a multi-program laboratory operated by Lockheed Martin Company, for the United States Department of Energy's National Nuclear Security Administration, under contract DE-AC04-94AL85000.

## References

[1] Fusion. Eng. Design 72 (2004) 1–326 (A large section of the "Special Issue on Innovative High-Power Density Concepts for Fusion Plasma Chambers" highlighted progress in this effort, and it continues as a primary focus of the Advanced Limiter/Divertor Plasma-Facing Components (ALPS) DOE program.).
[2] V.A. Evtikhin, et al., Plasma Phys. Control Fusion 44 (2002) 955 (and references therein).
[3] S.V. Mirnov, et al., J. Nucl. Mater. 390–391 (2009) 876.
[4] L.E. Zakharov, Fusion Eng. Des. 72 (2004) 149.
[5] H.W. Kugel, et al., J. Nucl. Mater. 363–365 (2007) 791.
[6] H.W. Kugel, et al., Phys. Plasmas 15 (2008) 056118.
[7] H.W. Kugel, et al., J. Nucl. Mater. 390–391 (2009) 1000.
[8] D. Mansfield, et al., J. Nucl. Mater. 390–391 (2009) 764 (and in this conference).
[9] R. Maingi, et al., Phys. Rev. Lett. 103 (2009) 075001.
[10] R. Majeski, et al., Phys. Rev. Lett. 97 (2006) 075002.
[11] R. Kaita, et al., Phys. Plasmas 14 (2007) 056111.
[12] M. Ono, et al., Nucl. Fusion 40 (2000) 557.
[13] M.G. Bell, et al., Plasma Phys. Control. Fusion 51 (2009) 124056.
[14] J.P. Allain, et al., J. Nucl. Mater. 390–391 (2009) 942.
[15] J.N. Brooks, et al., J. Nucl. Mater. 337–339 (2005) 1053.
[16] M.J. Baldwin, et al., Nucl. Fusion 42 (2002) 1318.
[17] H.W. Kugel, et al., Fusion Eng. Des. 84 (2009) 1125.
[18] R.E. Nygren, et al., Fusion Eng. Des. 84 (2009) 1438.
[19] W.R. Wampler, et al., J. Nucl. Mater. 390–391 (2009) 1009.
[20] D.K. Mansfield, et al., Phys. Plasmas 3 (1996) 1892.
[21] L.E. Zakharov, et al., J. Nucl. Mater. 363–365 (2007) 453.
[22] J.M. Canik, et al., Phys. Rev. Lett. 104 (2010) 045001.